ARTICLES

Ultrafast Dephasing of Photoexcited Polarons in Primary Doped Polyaniline

Jeongho Kim, Andreas -N. Unterreiner, Sachin Rane, Sungnam Park, Justin Jureller,† Lewis Book, Yish-Hann Liau, and Norbert F. Scherer*

Department of Chemistry, The James Franck Institute and Materials Research Science and Engineering Center, University of Chicago, 5735 S. Ellis Ave., Chicago, Illinois 60637

Received: April 4, 2002; In Final Form: September 10, 2002

Ultrashort pulse pump−probe and transient anisotropy methods are used to study polaron dynamics of primary doped conductive polyaniline in solution. The degenerate frequency pulses are resonant with the polaron absorption of the emeraldine salt form of polyaniline. Pronounced oscillatory components with frequencies of 160 and 210 cm^{-1} are observed, in good agreement with recent Raman and infrared spectral studies, and are likely to represent ground states modes. However, the close agreement with the excited state lifetime suggests that they may have partial excited state character. Photoexcited carrier dynamics have been identified on two distinct time scales. The very fast component, with a 34 fs exponential decay and 90% of the total amplitude, is attributed to the relaxation of the initially delocalized excitations within the polymer chain. This is supported by the transient anisotropy signal exhibiting a 30 fs Gaussian decay. In analogy with exciton dynamics in photosynthetic light harvesting assemblies, the extremely rapid anisotropy decay is attributed to dephasing of the initially delocalized polaron excitation due to diagonal disorder (i.e., variations in the monomer energies) and vibronic coupling. The longer time scale dynamics, occurring with two or more relaxations on >500 fs to >100 ps time scales, reflect the decay from the initially excited Franck−Condon region and the slow recovery of the ground state from a structurally altered, "twisted" intermediate. We propose this occurs by way of an electronic state with charge-separated character as in the isomerization of ethylenic species including retinal and PYP. Kinetic simulations are performed to establish a mechanism for the relaxation dynamics. Explicit inclusion of heterogeneity is necessary to adequately model the data.

I. Introduction

Polyaniline (PANI) is a conducting polymer with properties that are of fundamental interest and technological importance.[1] The electrical conductivity of polyaniline increases with the degree of doping with acids[2,3] resulting from improved one- and three-dimensional transport within the polymer film.[4] Presumably, the extent of structural variations and associated dislocations of the electronic structure and the degree of interchain contacts will affect the relative efficacy of intra- vs interchain transport.[5−9] Understanding the molecular-level aspects of the insulator-to-metal transition is, therefore, an important issue for improved performance. Ultrashort pulse methods have been of great utility for the investigation of molecular dynamics, including isomerization, following photoexcitation.[10] Several experiments with fs time resolution have been reported for the undoped emeraldine base form.[11−13] However, to date, there have not been any ultrafast measurements reported on the primary doped form of PANI.

Most of the properties of polyaniline can be linked to different oxidized and reduced states.[14] The electrical conductivity of the half-oxidized form, termed "emeraldine base", can be increased 10 orders of magnitude by acidification, a process termed primary doping. [Primary doping with acids protonates the monomer units of the polymer. The emeraldine base form of PANI, where 50% of the amine groups are oxidized, is fully protonated in the emeraldine salt form, which has the largest electrical conductivity.[2,3]] The primary doped form shows a broad absorption band centered at 806 nm (Figure 1) attributed to the formation of a polaron.[15,16] In this state, polyaniline is considered to be a quasi-1D conductor and the charge carriers

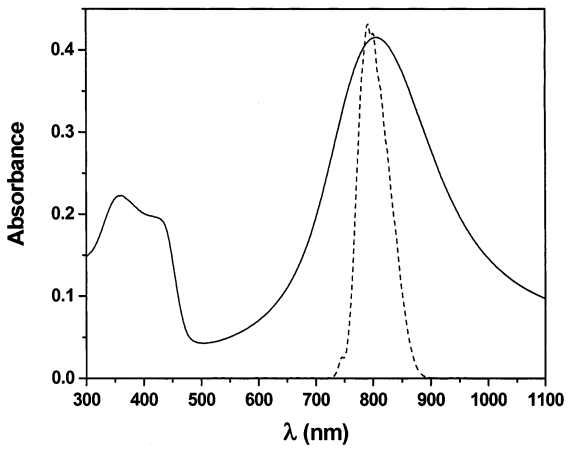

Figure 1. Absorption spectrum (solid) of polyaniline in chloroform and the laser spectrum (dashed) used in the pump−probe measurements.

* To whom correspondence should be addressed. E-mail: nfschere@uchicago.edu.
† NSF Predoctoral Fellow.

10.1021/jp020902h CCC: $22.00
Published on Web 11/19/2002

(i.e. polarons) can move along the polymer chain. Secondary doping induces further changes in the optical properties of polyaniline;[17,18] the absorption around 806 nm decreases, whereas a new absorption arises in the IR and the spectrum shows an isosbestic point around 1100 nm indicating conversion of material from one form to the other. [Secondary doping is an additional chemical treatment that increases electrical conductivity. As opposed to doping the material by adding charges (i.e., primary doping), one should view this process as solvation of the charges introduced by primary doping such that the polymer itself is not the only dielectric medium available for free energy stabilization.] The very broad IR band that ranges from 800 nm to beyond 2600 nm has been described as free carrier absorption; this occurs in conjunction with a very high specific conductivity of several hundred S/cm[19] in thin films.

The structural consequences of secondary doping have been followed by AFM studies of spin cast films.[20−22] An increase in the conductivity is accompanied by an uncoiling of the polymer chain where the morphologically rough polyaniline films become smooth and more continuous after secondary doping. The morphological studies on thin films were complemented with ultrafast pump−probe measurements of the decay of the photoexcited polaron.[20,21] The nonexponential (modeled as biexponential) dynamics could not be distinguished as originating from only intrachain or mixed intra- and interchain dynamics. Measurements on isolated polymer chains are required for comparison. This paper addresses this ambiguity through ultrafast pump−probe investigations of the primary doped conductive form of polyaniline. Pump−probe and anisotropy studies were performed exciting and probing the polymer dynamics associated with the polaron absorption band.

II. Experimental Section

A description of the laser has been published elsewhere.[23,24] Briefly, the home-built cavity-dumped laser system employed in these experiments delivered 18 fs pulses with center wavelengths of 800 nm to the solution samples. The 800 nm beam was split by a partial reflecting (50% R) mirror, and after prism precompensation for material dispersion, the two were used as pump and probe beams. The probe beam was attenuated 3-fold with a neutral density filter. A 25 cm focal length doublet lens was used to focus the pump and the probe beams in the sample, which was contained in a 0.5 mm path length spinning cell of 1″ diameter rotating at ∼10 Hz. The pump-induced probe transmission waveforms were dependent on the sample excitation rate. Above 200 kHz, a dip was observed preceding the rising edge of the signal near time zero, which was attributed to a thermal lensing effect, whereas the signal-to-noise ratio was reduced under 50 kHz. Thus, all of the experiments presented here were performed at 100 kHz and pump pulse energies of 1 nJ at the (focal plane of the) sample yielding a fluence of ∼20 μJ/cm^2, which can be considered to be in the low fluence regime for the study of metallic systems.[25] It was verified that the waveforms were independent of pump fluence over a 3-fold range above and below the operating point.

Data were acquired by detecting the probe beam transmission through the sample using a Si photodetector (New Focus, Nirvana 2007). The probe beam was split before the sample, and this reference beam was directed to an identical detector. The amplitudes of the probe and reference beams were adjusted to the same level with neutral density filters. The difference of the probe and reference signals was processed in a lock-in amplifier (Stanford Research, SR-830) referenced to a chopper at 2.5 kHz to give the AC component. The lock-in output was sampled by a 16-bit ADC (National Instruments) 1000 times at each delay step and the whole scan was repeated at least 50 times and averaged. The resultant was divided in the computer by the same reference signal sampled by the ADC (DC component) yielding $\Delta T/T$, the fractional change of the transmitted probe intensity induced by the pump pulse. This signal detection scheme was required to obtain the part in 10^6 sensitivity necessary for analysis. It was verified that the signal did not degrade for the 4 h data acquisition runs.

Anisotropy data were acquired by orienting a polarizer (Karl Lambrecht, MGTYA5) in the probe beam at 45° with respect to the pump beam. After the sample, the parallel and perpendicular components of the probe beam were separated by a Rochon polarizer (Karl Lambrecht, MRA-10). Each component was simultaneously detected with two identical Si photodetectors. The signals were then processed with two lock-in amplifiers, numerically averaged as described above and stored in the computer. It was verified that the initial anisotropy of the dye molecule IR-140 matched the expected value of 0.4 before and after the anisotropy measurement on PANI.

Polyaniline solutions were prepared by dissolving 0.1 g of emeraldine base powder (Polysciences, undoped form) in 10 mL of a chloroform solution containing 0.128 g D,L-camphorsulfonic acid. The solution was stirred and sonicated before filtering with a 200 nm pore size filter; larger pore sizes resulted in more scattered light from the sample and hence a worse signal-to-noise ratio. Sample aging leads to a change in the optical absorption spectrum because of complete development of the polaron band;[26] the small initial absorption around 730 nm decreases after several hours, and only the polaron band at 806 nm remains. Further sample aging results in the formation of aggregates. Therefore, the experiments presented here were performed on freshly prepared samples to avoid formation of aggregated particles yet after sufficient aging time (i.e., several hours) such that the polaron band was fully developed.

The linear absorption spectrum of a representative (primary doped) polyaniline solution used for pump−probe studies is shown in Figure 1, together with the laser spectrum of the pump and probe beams. Absorption spectra of the samples sealed in the spinning cells were measured before and after the ultrafast measurements. The spectra were unchanged, and the samples used here showed no tendency to aggregate; in fact, the spectra remained unchanged while stored in the cells for more than a week.

III. Results

The results presented here are divided into two parts: experiments on a long time scale, up to 100 ps, and a short time scale, up to 2 ps because signal relaxation occurs over more than 4 decades of time. Figure 2 shows the pump−probe signal of polyaniline solution in chloroform on a long time scale. The entire signal, still decaying at 100 ps, was fitted with a 4th order exponential decay with the parameters shown in Table 1 and a stretched exponential. As can be seen, the stretched exponential form gives a poorer fit to the data than the 4th order exponential although the two curves are very similar after several hundred femtoseconds time delay.

The short time pump−probe signal of polyaniline is shown in Figure 3. The autocorrelation trace, measured in a 100 μm thick BBO crystal, has been added for comparison.[27] Two major features can be seen: first, a very fast component that is clearly delayed from the autocorrelation trace and, second, the overall decay that is accompanied by oscillations. Two shorter exponential decay components with 34 and 560 fs time constants

TABLE 1: Nonlinear Least Squares Fit and LPSVD Analysis Results of the Pump−Probe Decay Signal Accompanied by Oscillations

	4th order exp. fit		3rd order exp. fit		LPSVD analysis			
component	amplitude ($\times 10^{-5}$)	τ (ps)	amplitude ($\times 10^{-5}$)	τ (ps)	amplitude ($\times 10^{-5}$)	freq (cm^{-1})	τ (ps)	phase (deg.)
1	0.9	117.0						
2	2.0	9.36	3.5	9.36	3.2	0	16.2	0
3	6.8	0.62	7.0	0.56	7.7	0	0.54	0
4	91	0.032	105	0.034	106	0	0.034	0
5					1.8	163	0.31	−29
6					0.4	219	0.55	−28

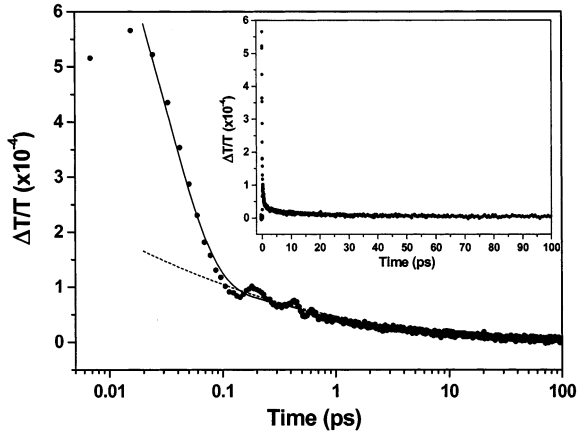

Figure 2. Pump-induced transient transmission (filled circles) with 4th order (solid line) and stretched exponential (dashed line) fits with logarithmic time axis. *Y* axis is transmission change divided by the probe beam DC intensity. The data were collected with a logarithmic time step to sample the large time range more efficiently. The decay was fitted with a 4th order exponential with the parameters in Table 1 and a stretched exponential with the form $S(t) = \Delta T/T = \alpha \exp[-(t/\tau)^{\beta}]$ with the best fit values of $\alpha = 1.81 \times 10^{-3}$, $\tau = 6.19 \times 10^{-6}$ ps, and $\beta = 0.108$. Inset is the same data on linear time axis.

are obtained when convoluting the instrument response function with a triexponential decay while fixing the long component at 9.36 ps, with the latter determined from the longer time range data of Figure 2. The oscillations were analyzed by linear prediction singular value decomposition (LPSVD) and Fourier transformation techniques;[28] Table 1 summarizes the parameters obtained by nonlinear least squares and LPSVD analysis. Figure 4 shows the spectra obtained by Fourier transformation of the residual (i.e., data minus triexponential fit) shown in Figure 3b. It shows the distinction between the Re(Fourier spectrum) vs the modulus spectrum. Note the distortion in the modulus (square root of the power spectrum) that arises from the "interference" of the dispersive (i.e., imaginary) part that shifts the small amplitude feature at 220 cm^{-1} to nearly 250 cm^{-1}. The real Fourier spectrum is the more appropriate representation of the actual molecular response. Both analyses resolve a dominant frequency component of 160 cm^{-1}. Also, a distinct peak centered at 210 cm^{-1} in the real part of the Fourier spectrum of Figure 4a can be related to the 218 cm^{-1} component in the LPSVD analysis. Some additional peaks between 300 and 600 cm^{-1} are evident, but the noise level of the data does not warrant further analysis.

The transient anisotropy was measured to further elucidate the origin of the decay components and the oscillations. The inset in Figure 5 shows the pump−probe transient responses, $S(t)$, obtained with parallel and perpendicular relative polarizations. The anisotropy, $r(t)$, is calculated from the transient transmission data, $S(t)$, as[29]

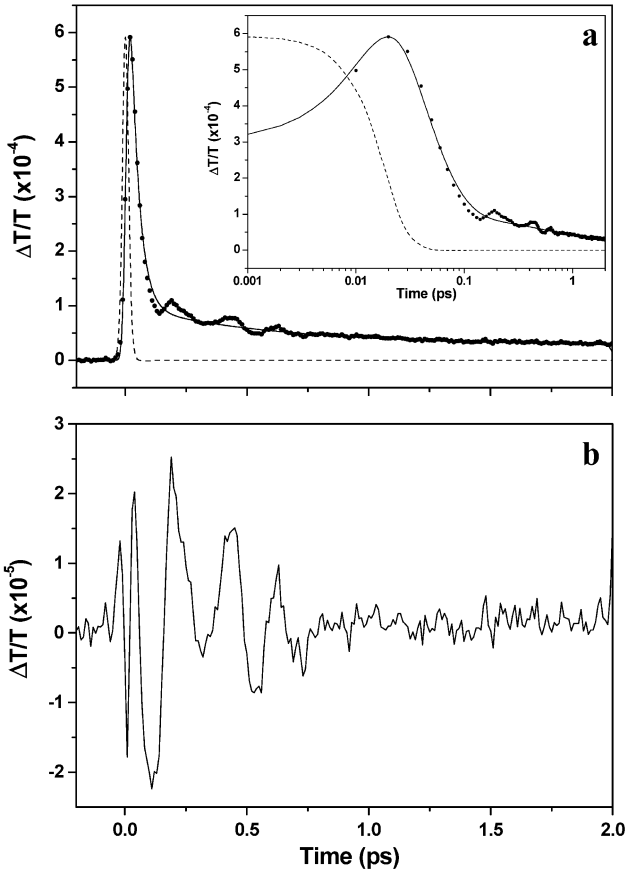

Figure 3. (a) Pump−probe signal (filled circles) and 3rd order exponential fit (solid line) convoluted with the instrument response function (dashed line) with the slow decay constant fixed at 9.36 ps (see text). The time step size is 10 fs. The fast decay component has a time constant of 34 fs, whereas the other slow component has a time constant of 562 fs. Inset is the same data, instrument response and fit on log time axis. (b) Residual obtained by subtracting the 3rd order exponential fit from the signal.

$$r(t) = \frac{S_{\parallel}(t) - S_{\perp}(t)}{S_{\parallel}(t) + 2S_{\perp}(t)} \tag{1}$$

The initial value of the transient anisotropy shown in Figure 5 is 0.26 and decreases within 60 fs to 0.14 and remains at this value for at least 0.4 ps; the anisotropy could not be examined for longer times because of the weakness of the signals. The initial anisotropy decay is fit much better by a Gaussian as opposed to exponential decay. A 30 fs fwhm Gaussian convoluted with the instrument response function is shown in Figure 5. There are oscillatory features with components of various frequencies, two of which are in the same frequency region as the dominant oscillations observed in the pump−probe signal.

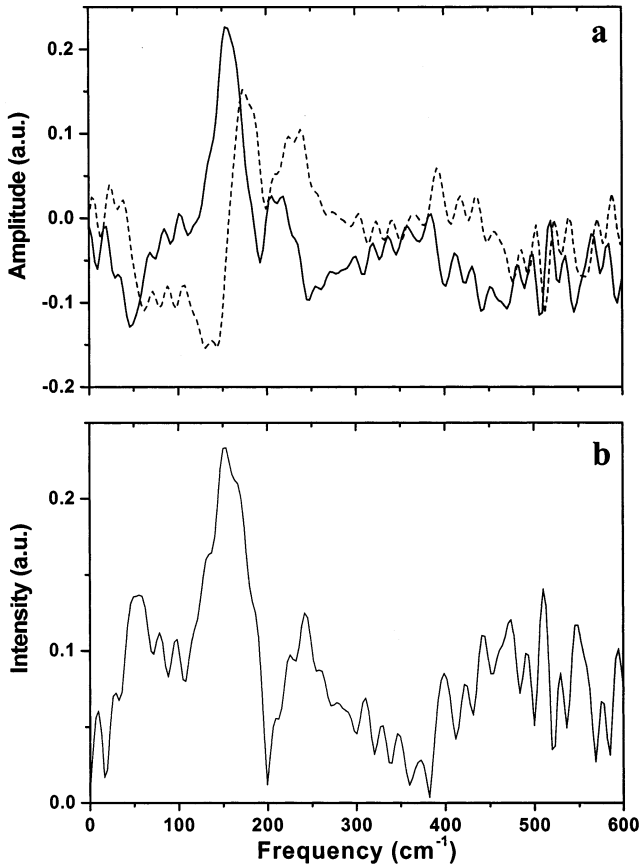

Figure 4. (a) Real (solid) and imaginary (dashed) Fourier spectra of the residual shown in Figure 3b. The spectra have been normalized to the Fourier spectrum of the temporal instrument (i.e., autocorrelation function) response. The Fourier transform for the transient transmission data was performed from −200 fs to 2 ps. (b) Fourier power spectrum of the residual.

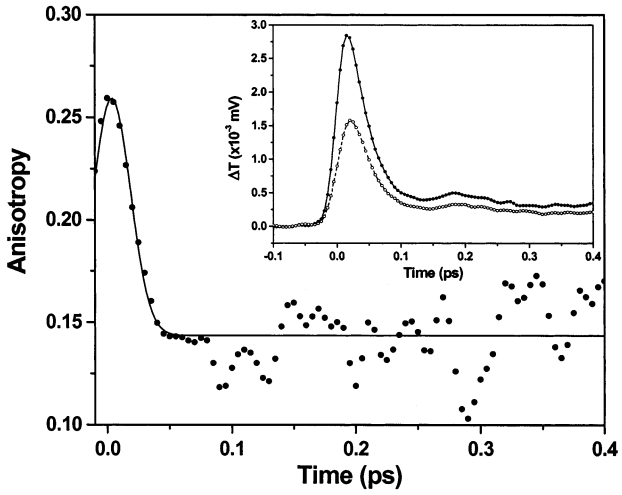

Figure 5. Anisotropy (filled circles) and Gaussian fit (solid line) with a width of 30 fs. The time step size is 5 fs. Inset is transient transmission data with the polarization of the probe beam parallel (solid line, filled circles) and perpendicular (dashed line, open circles) to the pump beam.[53]

IV. Discussion

Structural Inhomogeneity and Anisotropy Decay. In linear chain polymer systems, the excitation may migrate along the chain as a result of coupling between the regions.[30] If the chain is twisted, the excitation migration would lead to a change in the transition dipole orientation. Transient anisotropy measurements have been shown to be sensitive to ultrafast dephasing of collective excitations (e.g., excitons).[24,30] The anisotropy value reflects the degree of order of the transition dipole distribution in the polymer chain; a random distribution of transition dipole orientations would give $r(t) = 0$. Hochstrasser and co-workers demonstrated this behavior in polysilanes.[31] In the poly(phenylmethylsilane), the decay of the initial anisotropy from 0.4 to about 0.18 was found to occur with a 20−30 ps time constant, which is far slower than expected from the measured electronic bandwidth. Also, in an anisotropy measurement of poly(di-*n*-hexylsilane), the anisotropy decays from an initial value of 0.17 to 0.04 in 2−3 ps.[32] By contrast, in the present case for polyaniline, the anisotropy decays from an initial value of 0.26 to a final value of 0.14 within 60 fs, indicating stronger electron−phonon coupling than in polysilane. As pointed out by Cotts et al.,[31,33] torsional motion could result in restricted motion of the transition dipoles, which manifests itself in a plateau that is seen in the present experiments after 60 fs. The initial and final anisotropy values of 0.26 and 0.14, respectively, correspond to average angles of 29° and 40° for the transition dipoles.

Studies of exciton dynamics in photosynthetic light harvesting complexes have revealed a similar fast initial decay.[24] It was attributed to the localization of the transition dipole moment to random locations in the circular aggregate because of exciton dephasing. The initial exciton, delocalized over the ring aggregate, also gives rise to a large transition dipole moment that rapidly diminishes because of thermal fluctuations and energetic disorder among the monomers that randomize the phase relationships between the monomers. Similar phenomena could cause the fast decay of the polaron coherence observed here and the ∼30 fs initial decay of the pump−probe signal.

The Gaussian anisotropy decay can result from a distribution of transition energies in the polymer. A polaron can be delocalized only along a conjugated segment, so a distribution of polaron energies would result from the distribution of conjugated chain lengths. The latter are determined by chemical defects and structural disorder. Excitation localization by the (lower-energy) long-chain segments, with a distribution of transition dipole orientations, would cause the ultrafast decay of the anisotropy. This is in accord with the mechanism proposed to explain changes in the steady-state anisotropy with excitation wavelength.[31,34−36]

The low initial anisotropy value is also consistent with strong electron−phonon coupling and a large inhomogeneous distribution of polaron energies due to structural irregularities or defects. This is certainly possible given the broad line width shown in Figure 1. These factors can give rise to rapid exciton localization with a more randomized distribution of transition dipole moment orientations. Assuming a golden rule description of the rate of localization, one can scale the LH2 coupling to obtain a value for PANI. Because the rates for localization differ by about 4-fold, the electronic coupling would be 500−600 cm^{-1} in PANI.

Structural Changes Associated with Excitation and Relaxation. When polyaniline is photoexcited, it will evolve to a geometrically distorted structure by way of torsional motions between the adjacent benzenoid rings giving rise to a twisted geometry.[37] It was shown that the changes in the ring torsion angle play a crucial role in determining the energetics of the excited states of polyaniline.[38] Mode frequencies of 158 and 120 cm^{-1} were observed in IR and Raman spectra, respectively, of the emeraldine salt powder form.[37] Also, 213 and 200 cm^{-1} modes were observed in the same IR and Raman spectra,

TABLE 2: Best-Fit Parameters for Analysis of Kinetic Schemes

Scheme 1		Scheme 2		Scheme 3		Scheme 4	
$\chi^2 = 1.23 \times 10^{-7}$		$\chi^2 = 7.32 \times 10^{-8}$		$\chi^2 = 6.06 \times 10^{-8}$		$\chi^2 = 5.39 \times 10^{-8}$	
ϵ_{EG}	2.02×10^{-5}	ϵ_{EG}	3.10×10^{-5}	ϵ_{EG}	4.29×10^{-5}	ϵ_{EG}	5.17×10^{-5}
$1/k_1$(ps)	2.37	$[E_a]_0$	0.43	$1/k_{1a}$(ps)	0.66	$[E_a]_0$	0.47
$1/k_2$(ps)	40	$1/k_{1a}$(ps)	0.86	$1/k_{1b}$(ps)	1.38	$1/k_{1aa}$(ps)	0.71
		$1/k_{1b}$(ps)	0.91	$1/k_{2a}$(ps)	3.28	$1/k_{1ab}$(ps)	0.57
		$1/k_2$(ps)	11	$1/k_{2b}$(ps)	67	$1/k_{1ba}$(ps)	0.31
						$1/k_{1bb}$(ps)	3.26
						$1/k_{2a}$(ps)	1.63
						$1/k_{2b}$(ps)	24

respectively. These modes were assigned to torsional deformations of the $C_{ring}-N-C_{ring}$ units in the polymer chain with coupled ring motions; these could play an important role in the dynamics of exciton/polaron localization along the chain. Long-lived photoinduced absorption[39,40] and spins[41] were observed in the base form of polyaniline at low temperatures. These long-lived excitations were attributed to aggregation of polaron (or soliton) excitations because of the large number of rotated rings. These conformational changes would strongly localize the polarons and impede relaxation to the ground state.

The (exponential) decay observed in Figures 2 and 3 is accompanied by oscillations that relax with 310 or 550 fs time constants (see Table 1). The 160 cm^{-1} mode is the dominant frequency component with another mode at ~210 cm^{-1}. The 160 cm^{-1} feature was also identified in ultrashort pulse studies of primary doped polyaniline films.[21] It is most plausible to associate these oscillations to the ground state; these modes are strongly coupled to the electronic excitation and may be overdamped in the excited state because of the large amplitude conformational change. However, given the very similar values of the LPSVD time constants for the modes and excited-state lifetime obtained from kinetic modeling (see Tables 1 and 2), it is possible that the oscillations have contributions from excited-state vibrations.[42]

Given the torsional motions in the polymer chain, the oscillations in the anisotropy signal might reflect the fluctuation of transition dipole moment orientation. Fourier analysis of the data in Figure 5 reveals peaks near 200 cm^{-1} and also at higher frequencies. The large amplitude motions involved[37,38] could account for the present observation. Alternatively, the photoexcitation of a coherent superposition of electronically excited states in an inhomogeneously broadened band could give rise to the oscillations.[43] Further studies are required to settle this point.

The decay of the excitation must occur by a nonradiative channel as opposed to charge recombination that occurs in electroluminescent polymers such as PPV[44,45] and *trans*-polyacetylene[46] because the quantum yield for radiative emission from polyaniline is immeasurably small. Given the 100 ps bleach signal observed here, an intermediate state is necessary. This intermediate may involve a distorted geometrical structure and/or the photogeneration of quasi-free electrons.[18,21]

Kinetic Model of Relaxation. Kinetic modeling of the relaxation of the pump−probe signal was performed with several three-level kinetic schemes involving ground (G), excited (E), and intermediate (I) states. The four schemes shown in Figure 6 allow us to consider inhomogeneity in the kinetics of the excited and intermediate states. The associated kinetic equations were solved and the pump−probe signal was constructed from 0.2 to 100 ps considering ground-state bleaching and stimulated emission contributions. These equations are shown in the Appendix. The model signal was fitted to the measured signal using the Levenberg−Marquardt nonlinear least-squares fitting

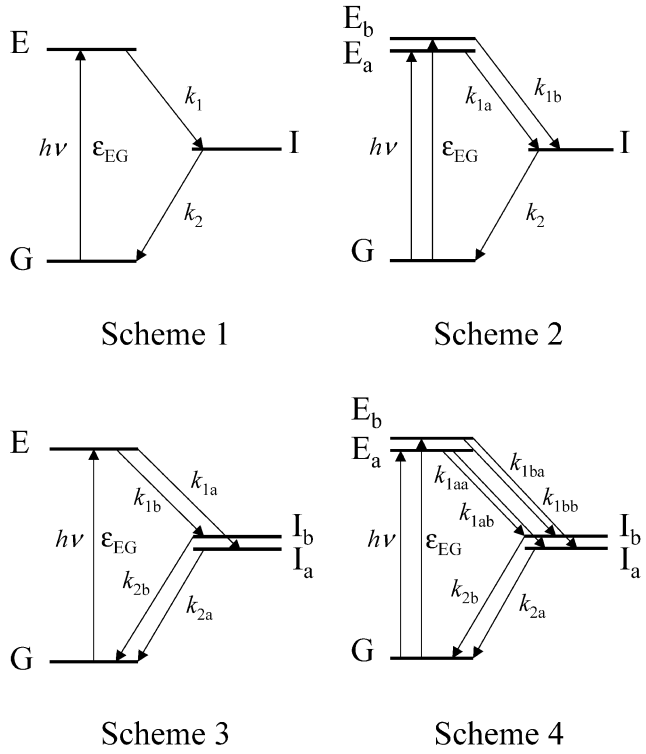

Figure 6. Kinetic schemes used to simulate the relaxation dynamics for a three-state system; ground (*G*), polaron (*E*), and optically "dark" intermediate (*I*). The *k*'s refer to the kinetic rate constants and ϵ_{EG} the effective extinction coefficient for the $E \leftarrow G$ optical transition. A multiplicity of states (e.g., E_a, E_b or I_a, I_b) allows modeling inhomogeneity in the kinetics.

algorithm[47] (MathSoft, Mathcad) by minimizing the sum of the squared deviations. The simulated signals and the best-fit parameters are shown in Figure 7 and Table 2, respectively. The initial dephasing was not included in the modeling so the first 200 fs was not included in the analysis.

The signals from Schemes 1 and 2 differ significantly from the measured pump−probe signal. Meanwhile, Scheme 3, in which the inhomogeneity of the intermediate state is considered, gives a reasonably close fit to the measured signal from 400 fs delay. Inhomogeneity of both the excited and intermediate states is considered in Scheme 4. This model gives a much better fit than the other three schemes, which could be a result of more parameters involved as suggested by the χ^2 values in Table 2. The time constants obtained from Schemes 3 and 4 show that the slow decay passes through the intermediate state "I_b" from which the decay to the ground state is much slower than from "I_a". This analysis supports the necessity of an intermediate state that exhibits inhomogeneous decay kinetics. This is substantiated by the success of the stretched exponential fit at times over 1 ps, as shown in Figure 2. The inhomogeneity may reflect structural "defects" that are associated with the polaron localization discussed above.

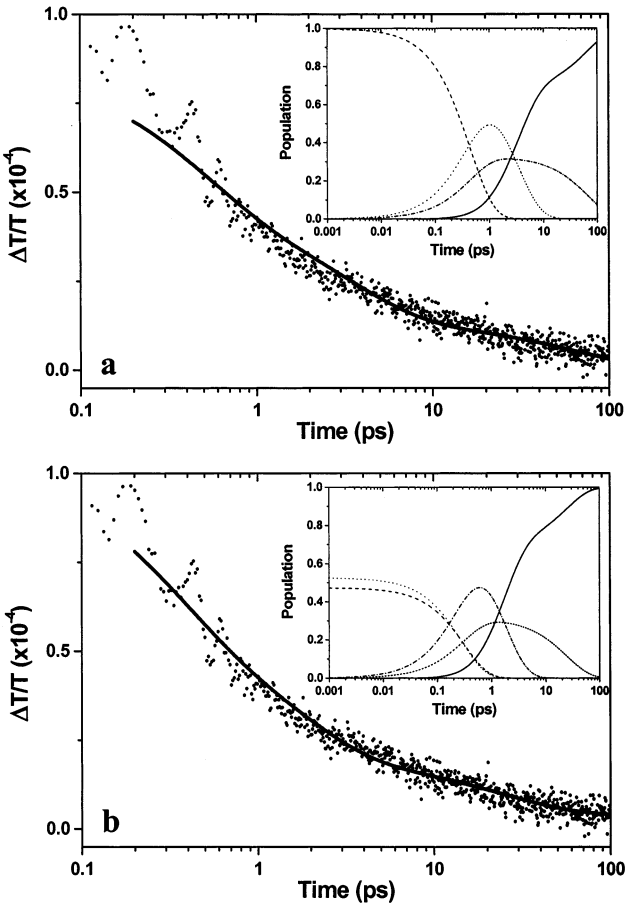

Figure 7. (a) Simulated signal (solid line) from Scheme 3 compared with the measured pump−probe signal (points). Inset is population evolution of the states involved in Scheme 3; G (solid), E (dashed), I_a (dotted), and I_b (dash−dotted). (b) Simulated signal (solid line) from Scheme 4 compared with the measured pump−probe signal. Inset is population evolution of the states involved in Scheme 4; G (solid), E_a (long-dashed), E_b (dotted), I_a (dash−dotted), and I_b (short-dashed).

Proposed Mechanism for Polaron Relaxation. Martinez and co-workers reported that the photoexcited state of ethylene rapidly evolves to a twisted geometry with charge-separated character that nonradiatively quenches to the ground state through a conical intersection.[48] This behavior is believed to be involved in the nonradiative ground recovery of ethylenic species, including ethylene, stilbene, retinal, GFP, and PYP.

Following this idea, we propose that the initial excitation in polyaniline relaxes nonradiatively to a "twisted" intermediate state with charge-separated character with subsequent "slow" ground state recovery over a broad range of time scales. The 34 fs exponential component reflects the fast relaxation dynamics of the initially delocalized polarons within an individual polymer chain. This is supported by the 30 fs Gaussian decay of the transient anisotropy signal. The long decay components, two or more exponential decays of >500 fs to >100 ps time constants, are attributed to the rapid relaxation from the initially excited Franck−Condon region and the slow recovery of the ground state via a long-lived intermediate state. Kinetic modeling shows the presence of long-lived intermediate states exhibiting significant inhomogeneity. As a matter of fact, a broad IR band is assigned to a free carrier absorption in secondary doped PANI.[18,21] Thus, time-resolved experiments in the near-infrared region would be essential to establish the free carrier contribution to the long time behavior.

V. Conclusions

Explicit modeling of the dynamics is important to understand the delocalization-to-localization transition and subsequent carrier transport.[49] Recent simulations and single molecule fluorescence studies suggest that conjugated polymers with chemical defects collapse into various conformations according to their stiffness.[50] They have shown that the anisotropy distribution obtained from polarization spectroscopy of MEH−PPV is consistent with a stiff polymer adopting a highly ordered conformation. Electronic structure calculations and analogous ultrafast nonlinear optical measurements to those presented here on aniline oligomers will be helpful in understanding the nature of the polaron and verifying the source of the initial dephasing. Ab initio calculations have been performed for aniline, *p*-phenylene diamine, and *N*,*N*′-bis(4′-aminophenyl)-1,4-quinonediimine.[51] Models of polyaniline with three and four aniline units have been used to identify size-dependent electronic properties of this polymer. Geometry optimization revealed the onset of helical structures even with di- and tri-aniline; it was suggested that one full turn of the helix is achieved with seven units.[52] The different oxidation states in the polymer, however, complicate simple scaling from the oligomer to the polymer unit. Nevertheless, a partially helical polymer structure that presents a distribution of localized exciton/polaron transition moment directions would explain the results of the anisotropy measurements reported herein.

Acknowledgment. This research was supported by the University of Chicago MRSEC (DMR-9808595) and the W. M. Keck Foundation (991705). Partial support for one of the laser systems used here was from the NIH (RO1-GM57768). N.F.S. acknowledges the Sloan and Dreyfus Foundations for fellowships. A.N.U. thanks the Deutsche Forschungsgemeinschaft (DFG) for a fellowship. We acknowledge helpful discussions with Prof. Todd Martinez and Prof. David Arnett.

Appendix

Because kinetic scheme 4 is not typically found in the literature, it is useful to summarize the pertinent equations. As shown in Figure 6, there are five states to consider with associated differential rate equations:

$$\frac{d[G]}{dt} = k_{2a}[I_a] + k_{2b}[I_b] \tag{A.1a}$$

$$\frac{d[E_a]}{dt} = -(k_{1aa} + k_{1ab})[E_a] \tag{A.1b}$$

$$\frac{d[E_b]}{dt} = -(k_{1ba} + k_{1bb})[E_b] \tag{A.1c}$$

$$\frac{d[I_a]}{dt} = k_{1aa}[E_a] + k_{1ba}[E_b] - k_{2a}[I_a] \tag{A.1d}$$

$$\frac{d[I_b]}{dt} = k_{1ab}[E_a] + k_{1bb}[E_b] - k_{2b}[I_b] \tag{A.1e}$$

These are solved with the boundary conditions at $t = 0$:

$$[G_0] = 0; \quad [E_a]_0 + [E_b]_0 = 1; \quad [I_a]_0 = [I_b]_0 = 0 \tag{A.2}$$

The resulting time-dependent populations for each state are

$$[E_a] = [E_a]_0 e^{-(k_{1aa}+k_{1ab})t} \quad \text{(A.3a)}$$

$$[E_b] = [E_b]_0 e^{-(k_{1ba}+k_{1bb})t} \quad \text{(A.3b)}$$

$$[I_a] = \frac{k_{1aa}}{k_{2a}-k_{1aa}-k_{1ab}}[E_a]_0\{e^{-(k_{1aa}+k_{1ab})t} - e^{-k_{2a}t}\} + \frac{k_{1ba}}{k_{2a}-k_{1ba}-k_{1bb}}[E_b]_0\{e^{-(k_{1ba}+k_{1bb})t} - e^{-k_{2a}t}\} \quad \text{(A.3c)}$$

$$[I_b] = \frac{k_{1ab}}{k_{2b}-k_{1aa}-k_{1ab}}[E_a]_0\{e^{-(k_{1aa}+k_{1ab})t} - e^{-k_{2b}t}\} + \frac{k_{1bb}}{k_{2b}-k_{1ba}-k_{1bb}}[E_b]_0\{e^{-(k_{1ba}+k_{1bb})t} - e^{-k_{2b}t}\} \quad \text{(A.3d)}$$

$$[G] = \frac{1}{k_{1aa}+k_{1ab}}\left(\frac{k_{1aa}k_{2a}}{k_{2a}-k_{1aa}-k_{1ab}} + \frac{k_{1ab}k_{2b}}{k_{2b}-k_{1aa}-k_{1ab}}\right) \times [E_a]_0\{1 - e^{-(k_{1aa}+k_{1ab})t}\} + \frac{1}{k_{1ba}+k_{1bb}}\left(\frac{k_{1ba}k_{2a}}{k_{2a}-k_{1ba}-k_{1bb}} + \frac{k_{1bb}k_{2b}}{k_{2b}-k_{1ba}-k_{1bb}}\right) \times [E_b]_0\{1 - e^{-(k_{1ba}+k_{1bb})t}\} + \left(\frac{k_{1aa}}{k_{2a}-k_{1aa}-k_{1ab}}[E_a]_0 + \frac{k_{1ba}}{k_{2a}-k_{1ba}-k_{1bb}}[E_b]_0\right) \times (e^{-k_{2a}t} - 1) + \left(\frac{k_{1ab}}{k_{2b}-k_{1aa}-k_{1ab}}[E_a]_0 + \frac{k_{1bb}}{k_{2b}-k_{1ba}-k_{1bb}}[E_b]_0\right) \times (e^{-k_{2b}t} - 1) \quad \text{(A.3e)}$$

Considering bleaching of the ground state (G) and stimulated emission from the excited state (E), the optical response, $S(t)$, can be constructed from eqs A.3a−e:

$$S(t) = \epsilon_{EG}(1 - [G]) + \epsilon_{EG}([E_a] + [E_b])$$

$$= \epsilon_{EG}\left[1 + [E_a]_0 e^{-(k_{1aa}+k_{1ab})t} + [E_b]_0 e^{-(k_{1ba}+k_{1bb})t} + \frac{1}{k_{1aa}+k_{1ab}}\left(\frac{k_{1aa}k_{2a}}{k_{2a}-k_{1aa}-k_{1ab}} + \frac{k_{1ab}k_{2b}}{k_{2b}-k_{1aa}-k_{1ab}}\right) \times [E_a]_0\{e^{-(k_{1aa}+k_{1ab})t} - 1\} + \frac{1}{k_{1ba}+k_{1bb}}\left(\frac{k_{1ba}k_{2a}}{k_{2a}-k_{1ba}-k_{1bb}} + \frac{k_{1bb}k_{2b}}{k_{2b}-k_{1ba}-k_{1bb}}\right) \times [E_b]_0\{e^{-(k_{1ba}+k_{1bb})t} - 1\} + \left(\frac{k_{1aa}}{k_{2a}-k_{1aa}-k_{1ab}}[E_a]_0 + \frac{k_{1ba}}{k_{2a}-k_{1ba}-k_{1bb}}[E_b]_0\right) \times (1 - e^{-k_{2a}t}) + \left(\frac{k_{1ab}}{k_{2b}-k_{1aa}-k_{1ab}}[E_a]_0 + \frac{k_{1bb}}{k_{2b}-k_{1ba}-k_{1bb}}[E_b]_0\right) \times (1 - e^{-k_{2b}t})\right] \quad \text{(A.4)}$$

The above equations and sloutions can be modified to obtain the analogous expressions for the other kinetic schemes. This requires imposing the following conditions:

SCHEME 1

$$[E_a] = [E]; \quad [E_b] = 0; \quad [I_a] = [I]; \quad [I_b] = 0 \quad \text{(A.5a)}$$

$$k_{1ab} = k_{1ba} = k_{1bb} = k_{2b} = 0; \quad k_{1aa} = k_1; \quad k_{2a} = k_2 \quad \text{(A.5b)}$$

SCHEME 2

$$[I_a] = [I]; \quad [I_b] = 0 \quad \text{(A.6a)}$$

$$k_{1ab} = k_{1bb} = k_{2b} = 0; \quad k_{1aa} = k_{1a}; \quad k_{1ba} = k_{1b}; \quad k_{2a} = k_2 \quad \text{(A.6b)}$$

SCHEME 3

$$[E_a] = [E]; \quad [E_b] = 0 \quad \text{(A.7a)}$$

$$k_{1ba} = k_{1bb} = 0; \quad k_{1aa} = k_{1a}; \quad k_{1ab} = k_{1b} \quad \text{(A.7b)}$$

References and Notes

(1) Epstein, A. J.; MacDiarmid, A. G. *Synth. Met.* **1995**, *69*, 179.

(2) MacDiarmid, A. G.; Chiang, J. C.; Halpern, M.; Huang, W. S.; Mu, S. L.; Somasiri, N. L. D.; Wu, W.; Yaniger, S. I. *Mol. Cryst. Liq. Cryst.* **1985**, *121*, 173.

(3) Kievelson, S.; Heeger, A. J. *Phys. Rev. Lett.* **1985**, *55*, 308.

(4) Joo, J.; Oh, E. J.; Min, G.; MacDiarmid, A. G.; Epstein, A. J. *Synth. Met.* **1995**, *69*, 251.

(5) Kohlman, R. S.; Joo, J.; Min, Y. G.; MacDiarmid, A. G.; Epstein, A. J. *Phys. Rev. Lett.* **1996**, *77*, 2766.

(6) Raghunathan, A.; Kahol, P. K.; McCormick, B. J. *Synth. Met.* **1999**, *100*, 205.

(7) Lee, K.; Heeger, A. J.; Cao, Y. *Synth. Met.* **1995**, *72*, 25.

(8) Lee, K.; Heeger, A. J. *Synth. Met.* **1997**, *84*, 715.

(9) Wang, Z. H.; Li, C.; Scherr, E. M.; MacDiarmid, A. G.; Epstein, A. J. *Phys. Rev. Lett.* **1991**, *66*, 1745.

(10) Schoenlein, R. W.; Peteanu, L. A.; Mathies, R. A.; Shank, C. V. *Science* **1991**, *254*, 412.

(11) Maciel, G. C.; de Araujo, C. B.; Correia, R. R. B.; de Azevedo, W. M. *Opt. Comm.* **1998**, *157*, 187.

(12) Hui, W.; Tianshu, L.; Weizhu, L.; Dang, M.; Meng, O.; Kecheng, G. *Chin. Phys. Lett.* **1994**, *11*, 491.

(13) Lin, W.-Z.; Wang, H.; Lai, T.-S.; Mo, D.; Ou, Y.-M.; Gong, K.-C. In *Ultrafast Phenomena IX*; Barbara, P. F., Knox, W. H., Mourou, G. A., Zewail, A. H., Eds.; Springer-Verlag: Berlin, 1994; Vol. 60, pp 322−324.

(14) Chiang, J. C.; MacDiarmid, A. G. *Synth. Met.* **1986**, *13*, 193.

(15) Stasfstrom, S.; Bredas, J. L.; Epstein, A. J.; Woo, H. S.; Tanner, D. B.; Huang, W. S.; MacDiarmid, A. G. *Phys. Rev. Lett.* **1987**, *59*, 1464.

(16) Makaruk, H. *Mod. Phys. Lett. B* **1995**, *9*, 543.

(17) MacDiarmid, A. G.; Epstein, A. J. *Synth. Met.* **1994**, *65*, 103.

(18) MacDiarmid, A. G.; Epstein, A. J. *Synth. Met.* **1995**, *69*, 85.

(19) S (Siemens) is the reciprocal of Ω ($1\ S = 1\ \Omega^{-1}$), and S/cm is the standard unit of conductivity.

(20) Feldstein, M. J.; Scherer, N. F. *Proc. SPIE* **1998**, *3272*, 58.

(21) Feldstein, M. J.; Zheng, W.; Liau, Y. H.; Rane, S.; Arnett, D.; MacDiarmid, A. G.; Scherer, N. F. *J. Phys. Chem.* **2002**, submitted.

(22) Rane, S.; Scherer, N. F. *J. Phys. Chem.* **2002**, submitted.

(23) Liau, Y.-H.; Unterreiner, A.-N.; Arnett, D. C.; Scherer, N. F. *Appl. Opt.* **1999**, *38*, 7386.

(24) Book, L. D.; Ostafin, A. E.; Ponomarenko, N.; Norris, J. R.; Scherer, N. F. *J. Phys. Chem. B* **2000**, *104*, 8295.

(25) Elsayed-Ali, H. E.; Juhasz, T.; Smith, G. O.; Bron, W. E. *Phys. Rev. B* **1991**, *43*, 4488.

(26) Zheng, W.; Min, Y.; MacDiarmid, A. G.; Angelopoulos, M.; Liao, Y. H.; Epstein, A. J. *Synth. Met.* **1997**, *84*, 109.

(27) The "thick" BBO crystal was used to better reflect the actual pump−probe instrument response and dispersion encountered over the interaction region in the sample.

(28) Vohringer, P.; Scherer, N. F. *J. Phys. Chem.* **1995**, *99*, 2684.

(29) Arnett, D. C.; Vohringer, P.; Scherer, N. F. *J. Am. Chem. Soc.* **1995**, *117*, 12262.

(30) Hochstrasser, R. M.; Pereira, M. A.; Share, P. E.; Sarisky, M. J.; Kim, Y. R.; Repinec, S. T.; Sension, R. J.; Thorne, J. R. G.; Iannone, M.; Diller, R.; Anfinrud, P. A.; Han, C.; Lian, T.; Locke, B. *Proc. Indian Acad. Sci. (Chem. Sci.)* **1991**, *103*, 351.

(31) Kim, Y. R.; Lee, M.; Thorne, J. R. G.; Hochstrasser, R. M.; Zeigler, J. M. *Chem. Phys. Lett.* **1988**, *145*, 75.

(32) Thorne, J. R. G.; Ohsako, Y.; Repinec, S. T.; Abrash, S. A.; Zeigler, J. M.; Hochstrasser, R. M. *J. Lumin.* **1990**, *45*, 295.

(33) Cotts, P. M.; Miller, R. D.; Trefonas, P. T., III.; West, R.; Fickes, G. N. *Macromolecules* **1987**, *20*, 1046.
(34) Johnson, G. E.; McGrane, K. M. *Polym.* **1986**, *27*, 352.
(35) Klingensmith, K. A.; Downing, J. W.; Miller, R. D.; Michl, J. *J. Am. Chem. Soc.* **1986**, *108*, 7438.
(36) Michl, J. *Polym.* **1987**, *28*, 420.
(37) Colomban, P.; Folch, S.; Gruger, A. *Macromolecules* **1999**, *32*, 3080.
(38) Ginder, J. M.; Epstein, A. J. *Phys. Rev. B* **1990**, *41*, 10674.
(39) McCall, R. P.; Ginder, J. M.; Leng, J. M.; Ye, H. J.; Manohar, S. K.; Masters, J. G.; Asturias, G. E.; MacDiarmid, A. G.; Epstein, A. J. *Phys. Rev. B* **1990**, *41*, 5202.
(40) Kim, K.; Blatchford, J. W.; Gustafson, T. L.; MacDiarmid, A. G.; Epstein, A. J. *Synth. Met.* **1995**, *69*, 247.
(41) Cromack, K.; Epstein, A. J.; Masters, J.; Sun, Y.; MacDiarmid, A. G. *Synth. Met.* **1991**, *41*−*43*, 641.
(42) Book, L. D.; Arnett, D. C.; Hu, H.; Scherer, N. F. *J. Phys. Chem.* **1998**, *102*, 4350.
(43) Arnett, D. C.; Moser, C. C.; Dutton, P. L.; Scherer, N. F. *J. Phys. Chem. B* **1999**, *103*, 2014.
(44) Sakamoto, A.; Nakamura, O.; Yoshimoto, G.; Tasumi, M. *J. Phys. Chem. A* **2000**, *104*, 4198.
(45) Burroughes, J. H.; Bradley, D. D. C.; Brown, A. R.; Marks, R. N.; Mackay, K.; Friend, R. H.; Burns, P. L.; Holmes, A. B. *Nature* **1990**, *347*, 539.
(46) Rothberg, L.; Jedju, T. M.; Townsend, P. D.; Etemad, S.; Baker, G. L. *Phys. Rev. Lett.* **1990**, *65*, 100.
(47) More, J. J.; Garbow, B. S.; Hillstrom, K. E. *User's Guide to Minpack I*; Argonne National Laboratory publication: Argonne, IL, 1980; Vols. 80−74.
(48) Ben-Nun, M.; Martinez, T. J. *Chem. Phys. Lett.* **1998**, *298*, 57.
(49) Mukamel, S.; Tretiak, S.; Wagersreiter, T.; Chernyak, V. *Science* **1997**, *277*, 781.
(50) Hu, D.; Yu, J.; Wong, K.; Bagchi, B.; Rossky, P.; Barbara, P. F. *Nature* **2000**, *405*, 1030.
(51) Jansen, S. A.; Doung, T.; Major, A.; Wei, Y.; Sein Jr., L. T. *Synth. Met.* **1999**, *105*, 107.
(52) Kwon, O.; McKee, M. *J. Phys. Chem. B* **2000**, *104*, 1686.
(53) Because of the detection scheme employed (see the Experimental Section), the shown signals are not normalized (ΔT). The parallel component was about half the level of prenormalized form of the pump−probe signal shown in Figures 2 and 3. Therefore, it was consistent with the pulse intensity conditions described in the Experimental Section.